Faceting instability in the presence of wetting interactions: A mechanism for the formation of quantum dots

A. A. Golovin, M. S. Levine, T. V. Savina, and S. H. Davis
Department of Engineering Sciences and Applied Mathematics, Northwestern University, Evanston, Illinois 60208-3100, USA
(Received 28 June 2004; revised manuscript received 11 October 2004; published 30 December 2004)

A mechanism for the formation of quantum dots on the surface of thin solid films is proposed, *not* associated with the Asaro-Tiller-Grinfeld instability caused by epitaxial stresses. This mechanism, free of stress, involves instability of the film surface due to strong anisotropy of the surface energy of the film, coupled to wetting interactions between the film and the substrate. According to the mechanism, the substrate induces the film growth in a certain crystallographic orientation. In the absence of wetting interactions with the substrate, due to a large surface-energy anisotropy, this orientation would be thermodynamically forbidden and the surface would undergo a long-wave faceting (spinodal decomposition) instability. We show that wetting interactions between the film and the substrate can suppress this instability and qualitatively change its spectrum, leading to the damping of long-wave perturbations and the selection of the preferred wavelength at the instability threshold. This creates a possibility for the formation of stable regular arrays of quantum dots even in the absence of epitaxial stresses. This possibility is investigated analytically and numerically, by solving the corresponding nonlinear evolution equation for the film surface profile, and analyzing the stability of patterns with different symmetries. It is shown that, near the instability threshold, the formation of stable hexagonal arrays of quantum dots is possible. With the increase of the supercriticality, a transition to a square array of dots or the formation of spatially localized dots can occur. Different models of wetting interactions between the film and the substrate are considered and the effects of the wetting potential anisotropy are discussed. It is argued that the mechanism can provide a new route for producing self-organized quantum dots.

DOI: 10.1103/PhysRevB.70.235342 PACS number(s): 68.65.Hb, 68.55.−a, 89.75.Kd

I. INTRODUCTION

The formation of quantum dots in epitaxially grown thin solid films has been attracting attention as a very promising area of nanotechnology that can lead to a new generation of electronic devices. It is generally understood that the main mechanism of the formation of quantum dots in thin solid films on solid substrates is the Asaro-Tiller-Grinfeld (ATG) instability[1] that releases epitaxial elastic stresses in the film caused by the crystal lattice mismatch between the film and the substrate.[2–5] At the same time, other mechanisms can also play an important role in the formation of surface structures during epitaxial growth, for example faceting instability of a thermodynamically unstable surface caused by strong surface-energy anisotropy[6,7] or slope-dependent surface currents caused by the Schwöbel effect.[8–10]

The characteristic feature of these mechanisms is that they produce long-wave instabilities of the film surface leading to the formation of mounds that usually coarsen, with larger islands growing at the expense of the smaller ones.[11] At the same time formation of a system of islands with almost uniform sizes has been also observed.[12] Several mechanisms that can terminate the coarsening process have been identified. For example, a balance between the surface and elastic energies can lead to the formation of uniform-size islands as a preferred configuration having minimal energy.[2,13] Another, dynamic mechanism is associated with the normal growth of the interface, e.g., by evaporation-condensation or due to the presence of a diffusion boundary layer typical of chemical vapor deposition. The normal growth introduces convective effects in the evolution of the interface that compete with the coarsening process by sustaining ridges and corners of faceted mounds.[7,14,15] However, when the growth stops, further annealing will cause coarsening of the surface structures. Recently, an additional mechanism that can terminate coarsening of the surface structures has been identified. This mechanism is based on wetting interactions between the film and the substrate.[16,17] It has been shown that wetting interactions can change the spectrum of the ATG instability,[18,16,19] or surface instability caused by the Schwöbel effect,[20] and lead to the selection of a finite wavelength near the instability threshold and therefore to the possibility of the formation of permanent spatially regular patterns.[16] In this case spatially regular arrays of dots (or pits) are formed as a result of nonlinear dynamics near the instability threshold and the corresponding steady state can be considered as having a local energy minimum. So far the formation of spatially regular arrays of dots has been investigated for the case of ATG instability accompanied by wetting interactions between the film and the substrate.[16,17] The interplay between the film-substrate wetting interactions and *faceting instability*, caused by anisotropic surface energy, has not been studied yet. In this paper we investigate this coupling and show that, even in the absence of epitaxial stresses, wetting interactions can terminate coarsening and lead to the formation of permanent regular arrays of quantum dots, as well as spatially localized dots, thus providing a new route for quantum-dot fabrication.

II. PROBLEM STATEMENT

Consider a thin, solid film grown on a solid substrate where the lattice mismatch between the two materials is neg-

ligible, the surface energy γ of the film is strongly anisotropic, the film wets the substrate and it is thin enough for the wetting interaction energy to affect the chemical potential of the film.

Let us assume that the substrate determines the initial crystallographic orientation of the free surface of a growing film. Let us also assume that *in the absence of the substrate*, or when the film is thick enough so it does not "feel" the substrate, this orientation would be in the range of "forbidden orientations."

In this paper we consider only high-symmetry orientations, such as [001] and [111]. In this case, the forbidden orientation of the growing surface implies that the surface-stiffness tensor,[21,22]

$$\tilde{\gamma}_{\alpha\beta} = \gamma\delta_{\alpha\beta} + \frac{\partial^2\gamma}{\partial\theta_\alpha\partial\theta_\beta}, \tag{1}$$

is diagonal for this orientation and has two equal negative components,

$$\tilde{\gamma}_{11} = \tilde{\gamma}_{22} \equiv -\sigma < 0. \tag{2}$$

(Here $\theta_{\alpha,\beta}$ are the surface angular coordinates and $\delta_{\alpha\beta}$ is the Kroneker delta.) In the absence of wetting interactions between the film and the substrate, such a surface is thermodynamically unstable and exhibits spontaneous formation of pyramidal "faceted" structures that coarsen in time.[7,15] The film would decompose into faceted islands and exhibit the Volmer-Weber growth, rather than the Stranski-Krastanov one. However, as we show below, the presence of wetting interactions can *suppress* this instability, or qualitatively change it, so that it would lead to the Stranski-Krastanov growth in the form of spatially regular arrays of islands.

The continuum evolution of the film free surface can be described by the classical surface-diffusion equation,

$$v_n = \mathcal{D}\Delta_s\mu, \tag{3}$$

where v_n is the normal surface velocity, $\mathcal{D} = D_S S_0 \Omega_0 V_0/(RT)$[23] ($D_S$ is the surface diffusivity, S_0 is the number of atoms per unit area on the surface, Ω_0 is the atomic volume, V_0 is the molar volume of lattice cites in the film, R is the universal gas constant and T is the absolute temperature), Δ_s is the surface Laplace operator and the chemical potential

$$\mu = \frac{\delta\mathcal{F}}{\delta h}, \tag{4}$$

where $\mathcal{F}$ is the free energy functional and $h(x,y,t)$ is the shape of the film surface. In the *absence* of elastic stresses and wetting interactions between the film and the substrate,

$$\mathcal{F} = \int \left[\mu_0 h + I(h_x,h_y) + \tfrac{1}{2}\nu(\Delta h)^2\right]dxdy, \tag{5}$$

where μ_0 is the volume part of the free energy (μ_0 is the constant chemical potential of a planar film), $I = \gamma(h_x,h_y)\sqrt{1+(\nabla h)^2}$ is the weighted anisotropic surface energy that depends on the local surface slope, and ν is the regularization coefficient that measures the energy of edges and corners[6,7,24] (for simplicity, we write this term here in the small-slope approximation that will be further employed in this paper). The free energy (5) gives the chemical potential

$$\mu = \mu_0 + \mu_\gamma \equiv \mu_0 + \tilde{\gamma}_{\alpha\beta}C_{\alpha\beta} + \nu\Delta^2 h, \tag{6}$$

where $C_{\alpha\beta}$ is the surface curvature tensor.

In the presence of wetting interactions between the film and the substrate, the film chemical potential μ strongly depends on the film thickness h for $h \sim \delta_w$, where δ_w is the characteristic wetting length, and $\mu \to \mu_0$ for $h \gg \delta_w$. In this case the film free energy can be written as

$$\mathcal{F} = \int \left[f(h,h_x,h_y) + \tfrac{1}{2}\nu(\Delta h)^2\right]dxdy, \tag{7}$$

where $f(h,h_x,h_y) \to \mu_0 h + I(h_x,h_y)$ for $h \gg \delta_w$. The *wetting* part of the free energy can be then defined as

$$\mathcal{F}_w = \int [f(h,h_x,h_y) - \mu_0 h - I(h_x,h_y)]dxdy. \tag{8}$$

In this paper, we consider the following two models for wetting interactions between the film and the substrate.

A *two-layer wetting model*, according to which the wetting interactions between the film and the substrate are described as a thickness-dependent surface energy of the film, $\gamma(h)$. This dependence is usually taken to be[25]

$$\gamma(h) = \gamma_f + (\gamma_s - \gamma_f)\exp(-h/\delta), \tag{9}$$

where γ_s=const is the surface energy of the substrate in the absence of the film, γ_f is the energy of the film free surface far from the substrate, and δ is the characteristic wetting length. This model is consistent with *ab initio* calculations.[26,27] For anisotropic surface energy of the film,

$$\gamma_f = \gamma_f^0[1 + \varepsilon(h_x,h_y)], \tag{10}$$

where γ_f^0=const and $\varepsilon(h_x,h_y)$ is the anisotropy function that depends on the orientation of the film surface. Thus, in this model the free energy density in (7) is $f(h,h_x,h_y) = \gamma(h,h_x,h_y)\sqrt{1+|\nabla h|^2}$, and the chemical potential is computed as $\mu = \mu_\gamma + \mu_w$, where μ_γ is defined by (6) and

$$\mu_w = \frac{\dfrac{\partial\gamma}{\partial h} - \left[\dfrac{\partial^2\gamma}{\partial h\partial h_x}h_x + \dfrac{\partial^2\gamma}{\partial h\partial h_y}h_y\right](1+|\nabla h|^2)}{\sqrt{1+|\nabla h|^2}}. \tag{11}$$

Note that in this case $\tilde{\gamma}_{\alpha\beta}$ in μ_γ depends on h.

A *glued wetting-layer model*, that considers isotropic wetting free energy, additive to the anisotropic surface energy, yielding $\mu = \mu_\gamma + \mu_w$, with μ_γ defined by (6) and μ_w being an exponentially decaying function of h that has a singularity at $h \to 0$:

$$\mu_w = -w(h/\delta)^{-\alpha_w}\exp(-h/\delta). \tag{12}$$

Here δ is the characteristic wetting length, $w > 0$ characterizes the "strength" of the wetting interactions, and $\alpha_w > 0$ characterizes the singularity of the wetting potential at $h \to 0$. This singularity is a simple continuum phenomenological model of a very large potential barrier for removal of an ultra-thin (possibly monolayer) wetting layer that persists be-

tween surface mounds during Stranski-Krastanov growth process (see also Refs. 20, 28, and 29). We are not aware of experimental studies in which the wetting interaction potential has been measured and the glued wetting-layer model is a reasonable approximation for the purpose of our analysis.

Thus, in the small-slope approximation and for high-symmetry orientations, the surface chemical potential in both of these models have the same form,

$$\mu = \mu_\gamma^0 + \mu_w, \tag{13}$$

where $\mu_\gamma^0 = \mu_\gamma(h_0)$ is defined by (6) and evaluated at the initial film thickness h_0, and the part of chemical potential due to wetting can be expanded as

$$\mu_w = W_0(h) + W_2(h)(\nabla h)^2 + W_3(h)\nabla^2 h + \cdots, \tag{14}$$

where $W_{0,2,3}(h)$ are smooth functions, rapidly (exponentially) decaying with the increase of h, $W_3(h_0)=0$, and $2W_2 = dW_3/dh$ [due to (4)].

In the small-slope approximation, and in the particular cases of high-symmetry orientations ([001] or [111]) of a crystal with cubic symmetry, the evolution equation (3) for the film thickness can be written in the following form:

$$\partial_t h = \mathcal{D}\Delta[\sigma\Delta h + \nu\Delta^2 h - \Gamma_{ijk}[h] + W_0(h) + W_2(h)(\nabla h)^2 + W_3(h)\Delta h], \tag{15}$$

where for the orientations [001] and [111] the nonlinear differential operator $\Gamma_{ijk}[h]$ has the following forms,[7] respectively:

$$\Gamma_{001} = (ah_x^2 + bh_y^2)h_{xx} + (bh_x^2 + ah_y^2)h_{yy} + 4bh_x h_y h_{xy}, \tag{16}$$

$$\Gamma_{111} = a[h_x^2 h_{xx} + h_y^2 h_{yy} + 2h_x h_y h_{xy}] + \frac{a}{3}[h_y^2 h_{xx} + h_x^2 h_{yy} - 2h_x h_y h_{xy}] + b[(h_{xx} - h_{yy})h_y + 2h_{xy}h_x]. \tag{17}$$

Here the coefficients a and b characterize the surface-energy anisotropy and can be computed from the surface-energy dependence on the surface orientation. Naturally, the nonlinear operator Γ_{001} is invariant with respect to rotations by $\pi/2$, as well as any of the transformations $x\to -x$, $y\to -y$, $x\to y$, while Γ_{111} is invariant with respect to rotations by $2\pi/3$ as well as the transformation $y\to -y$, $b\to -b$. The functions $W_{0,2,3}(h)$ are determined by the type of a wetting interaction model and can also differ for different orientations of the film surface.

Note that Eq. (15) with the nonlinear operators Γ_{ijk} defined by (16) and (17) can be written in a variational form

$$\partial_t h = \mathcal{D}\nabla^2 \frac{\delta \mathcal{F}}{\delta h}, \tag{18}$$

where $\mathcal{F}=\int F dxdy$, and the free energy density

$$F = -\frac{\sigma}{2}(\nabla h)^2 + \frac{\nu}{2}(\Delta h)^2 + \mathcal{G}_{ijk} + \int W_0(h)dh - \frac{1}{2}W_2(h)(\nabla h)^2, \tag{19}$$

with

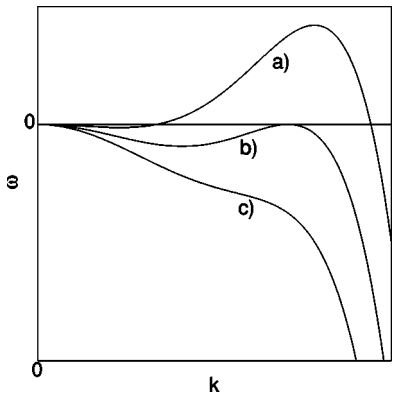

FIG. 1. Sketch of dispersion curves defined by (22) for (a) $\sigma^2/(4\nu W_{01})>1$, (b) $\sigma^2/(4\nu W_{01})=1$, and (c) $\sigma^2/(4\nu W_{01})<1$.

$$\mathcal{G}_{001} = \frac{a}{12}(h_x^4 + h_y^4) + \frac{b}{2}h_x^2 h_y^2, \tag{20}$$

$$\mathcal{G}_{111} = \frac{a}{12}(\nabla h)^4 + \frac{b}{6}(3h_x^2 h_y - h_y^3). \tag{21}$$

In the following sections we investigate the stability and nonlinear dynamics of the solid-film surface governed by Eq. (15).

III. FACETING INSTABILITY IN THE PRESENCE OF WETTING INTERACTIONS

Consider infinitesimal perturbations of a planar film surface, $h=h_0+\tilde{h}e^{i\mathbf{k}\cdot\mathbf{x}+\omega t}$, and linearize Eq. (15) to obtain the following dispersion relation between the perturbation growth rate ω and the wave vector $\mathbf{k}$:

$$\omega = \mathcal{D}(-W_{01}k^2 + \sigma k^4 - \nu k^6), \tag{22}$$

where $k=|\mathbf{k}|$ and

$$W_{01} = \left(\frac{\partial W_0}{\partial h}\right)_{h=h_0}. \tag{23}$$

One can see that if the film wets the substrate, i.e., when $W_{01}>0$, the wetting interactions suppress the long-wave faceting instability caused by the surface-energy anisotropy. The instability occurs only for

$$\frac{\sigma^2}{4\nu W_{01}} > 1, \tag{24}$$

i.e., if either the wetting interaction is less than the threshold value, $W_{01}<W_{01}^c=\sigma^2/(4\nu)$, or the surface stiffness is larger than the threshold value, $\sigma>\sigma_c=2\sqrt{W_{01}\nu}$. At the instability threshold, the wavelength of the unstable perturbations λ is *finite*, $\lambda=\lambda_c=2\pi/k_c$, where

$$k_c = \sqrt{\frac{\sigma}{2\nu}}. \tag{25}$$

Typical dispersion curves defined by (22) are schematically shown in Fig. 1. Note that the critical wave number at the

threshold does not depend on the wetting potential and is determined only by the surface stiffness and the energy of edges and corners. For the parameter values typical of semiconductors like Si or Ge, with the surface energy $\gamma \sim 2.0\ \mathrm{J\,m^{-2}}$, surface stiffness $\sigma \sim 0.2\ \mathrm{J\,m^{-2}}$, the lattice spacing $a_0 \sim 0.5$ nm and the regularization parameter $\nu \sim \gamma a_0^2 \sim 5.0 \times 10^{-19}$ J, the wavelength of the structure at the onset of instability is 14.0 nm.

Thus, in the presence of the wetting interactions with the substrate, the faceting instability becomes *short wave*. This is qualitatively different from the case of the faceting instability in the absence of the wetting interactions when the instability is *long wave*, i.e., when all perturbations whose wavelengths are larger than a certain threshold are unstable. In other words, wetting interactions with the substrate change the faceting instability from the spinodal decomposition type[6] to the Turing type,[30] thus leading to the possibility of changing the system evolution from Ostwald ripening (coarsening) to the formation of spatially regular patterns. The latter is studied in the following sections.

IV. FORMATION OF SURFACE STRUCTURES: 1+1 CASE

In this section we investigate the nonlinear evolution of surface structures resulting from the faceting instability in the presence of wetting interactions with the substrate in a 1+1 case of a two-dimensional film with a one-dimensional surface. In this case, the evolution equation (15) for the shape of the film surface, after the rescaling $x \to (\nu/\sigma)^{1/2} x$, $t \to [\nu^2/(\mathcal{D}\sigma^3)]t$, $h \to (\nu/a)^{1/2} h$, becomes

$$\partial_t h = [h_{xx} + h_{xxxx} - h_x^2 h_{xx} + w_0(h) + w_2(h) h_x^2 + w_3(h) h_{xx}]_{xx}, \tag{26}$$

where $w_{0,2,3}(h)$ are the rescaled functions $W_{0,2,3}(h)$, respectively [$w_3(h_0)=0$, $2w_2 = dw_3/dh$]. In this scaling, the instability occurs for $(\partial w_0/\partial h)_{h=h_0} \equiv w_{01} < \frac{1}{4}$ at the wave number $k_c = \sqrt{2}/2$.

First, we investigate the evolution near the instability threshold by means of weakly nonlinear analysis, and then we study a strongly nonlinear evolution by means of numerical simulations.

A. Weakly nonlinear analysis

Consider $w_{01} = \frac{1}{4} - 2\epsilon^2$, $\epsilon \ll 1$, introduce the long-scale coordinate $X = \epsilon x$ and the slow time $T = \epsilon^2 t$, and expand

$$\tilde{h} = h - h_0 = \epsilon[A(X,T)e^{ik_c x} + \text{c.c.}] + \epsilon^2[A_2(X,T)e^{2ik_c x} + B(X,T) + \text{c.c.}] + \cdots, \tag{27}$$

$$w_0(h) = w_{00} + w_{01}\tilde{h} + w_{02}\tilde{h}^2 + w_{03}\tilde{h}^3 + \cdots, \tag{28}$$

$$w_2(h) = w_{20} + w_{21}\tilde{h} + \cdots, \tag{29}$$

$$w_3(h) = w_{31}\tilde{h} + w_{32}\tilde{h}^2 + \cdots, \tag{30}$$

where $w_{31} = 2w_{20}$ and $w_{32} = w_{21}$. Substitute (27)–(30) into Eq. (26) to obtain the corresponding problems in the successive orders of ϵ. From the problem at second order one finds

$$A_2 = \tfrac{2}{9}(3w_{20} - 2w_{02})A^2. \tag{31}$$

As the solvability condition at the third order, one obtains the evolution equation for the complex amplitude of the unstable, spatially periodic mode, $A(X,T)$. The solvability condition at the fourth order yields the evolution equation for the real amplitude $B(X,T)$ of the Goldstone (zero) mode associated with the conservation of mass. Together, the two equations form the following system of coupled equations:

$$A_T = A + A_{XX} - \lambda_0 |A|^2 A + sAB,$$

$$B_T = \tfrac{1}{4} B_{XX} - 2s(|A|^2)_{XX}, \tag{32}$$

where

$$\lambda_0 = \tfrac{1}{8} - \tfrac{1}{9}(3w_{20} - 2w_{02})^2 - \tfrac{1}{2}w_{21} + \tfrac{3}{2}w_{03}, \tag{33}$$

$$s = \tfrac{1}{2}w_{20} - w_{02}. \tag{34}$$

The system of amplitude equations (32) has a stable, stationary solution, $A = \lambda_0^{-1/2}$, $B = 0$, corresponding to spatially periodic pattern (array of dots), if[31,16]

$$\lambda_0 > 8s^2 = 2(w_{20} - 2w_{02})^2. \tag{35}$$

Condition (35) defines a region in the parameter space in which one can observe the formation of stable periodic arrays of dots. First, consider a *glued-layer* wetting potential defined by (12). From (24) one obtains that the planar film surface becomes unstable with respect to periodic structures for

$$-\frac{\sigma^2 \delta}{w\nu} > 4(\alpha_w + \zeta)\zeta^{-(\alpha_w+1)} e^{-\zeta}, \tag{36}$$

where $\zeta = h_0/\delta$. Since for the wetting potential (12) $w_2(h) = w_3(h) \equiv 0$, one obtains from (35) and (36) that a near-threshold periodic surface structure is stable if

$$\frac{a\delta^2}{\nu} > f(\zeta, \alpha_w), \tag{37}$$

where

$$f(\zeta,\alpha_w) = [18\zeta^2(\zeta+\alpha_w)^2]^{-1}[10\zeta^4 + 40\alpha_w\zeta^3 + \alpha_w(11+60\alpha_w)\zeta^2 + 2\alpha_w(20\alpha_w^2 + 11\alpha_w - 9)\zeta + \alpha_w^2(10\alpha_w^2 + 11\alpha_w + 1)]. \tag{38}$$

Conditions (36) and (37) are shown in Fig. 2.

Now consider a *two-layer* wetting potential defined by (9) with

$$\gamma_f = \gamma_f^0[1 + \varepsilon \cos 4(\theta_0 + \theta)], \tag{39}$$

where $\theta = \arctan(h_x)$ and θ_0 corresponds to the orientation of the planar surface of the film, parallel to the substrate; for the high-symmetry orientations [01] and [11], $\theta_0 = 0$, $\pi/4$, respectively. It is convenient to introduce the following dimensionless parameters:

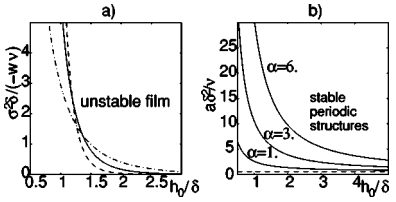

FIG. 2. (a) Parameter regions where a planar film surface is unstable (above the corresponding curves) for $\alpha_w=6.0$ (dashed line), $\alpha_w=3.0$ (solid line) and $\alpha_w=1.0$ (dashed-dotted line). (b) Parameter regions where weakly nonlinear periodic surface structures are stable (above the corresponding curves) for different values of α_w.

$$\Gamma=\frac{\gamma_{f0}}{\gamma_s}(15\varepsilon-1),\quad \zeta=\frac{h_0}{\delta},\quad \tilde{\varepsilon}_1=\frac{\varepsilon+1}{15\varepsilon-1},\quad \tilde{\varepsilon}_2=\frac{95\varepsilon-1}{15\varepsilon-1}.$$

The film wets the substrate if $\Gamma<\tilde{\varepsilon}_1^{-1}$ or $\gamma_s/\gamma_{f0}>\varepsilon+1$. In this case, the nonlinear anisotropy coefficient a in Eq. (15) is always positive. The faceting instability requires a negative surface stiffness that can be achieved only if $15\varepsilon-1>0$, and

$$\zeta>\ln(1+\Gamma^{-1}). \tag{40}$$

The instability threshold condition (24) gives

$$\frac{\gamma_s\delta^2}{\nu}\geqslant\frac{4e^{\zeta}[1-\Gamma\tilde{\varepsilon}_1]}{[\Gamma(e^{\zeta}-1)-1]^2}. \tag{41}$$

The analysis of the conditions (40) and (41) shows that the short-wave instability of the film surface that can lead to pattern formation can occur only if the film thickness is above a threshold value determined only by the surface-energy anisotropy and the wetting length, namely, for

$$h_0>\delta\ln\left[\frac{16\varepsilon}{15\varepsilon-1}\right]. \tag{42}$$

Using (35) one can show that the weakly nonlinear periodic structure is stable if

$$\frac{\gamma_s\delta^2}{\nu}>f(\zeta,\Gamma,\varepsilon), \tag{43}$$

where

$$f=\frac{2}{27}\frac{\Gamma^2(5e^{2\zeta}+14e^{\zeta}+35)+14\Gamma(e^{\zeta}+5)+35}{e^{-\zeta}[\Gamma(e^{\zeta}-1)-1]^2[\tilde{\varepsilon}_2\Gamma(e^{\zeta}-1)-1]}. \tag{44}$$

The conditions (40)–(44) allow one to determine regions in the (Γ,ζ) parameter plane where spatially regular surface structures can occur as a result of thermodynamic instability of the film surface caused by strongly anisotropic surface-tension in the presence of wetting interaction described by the two-layer model (9). Examples of these regions for different values of the anisotropy parameter ε are shown in Fig. 3.

Solid lines correspond to the condition (41), the dashed lines correspond to the condition (44). The film is unstable in the regions above the solid lines, and the stable periodic structures can form in the region near the solid line which lies above the dashed curve. One can see that for given values of the surface-energy anisotropy, ε, and the value of $\gamma_s\delta/\nu$, the formation of stable periodic structures occurs if the ratio of the initial film thickness to the wetting length is within a certain interval.

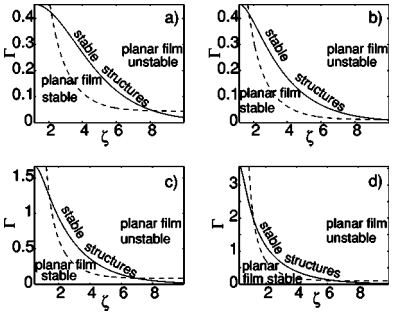

FIG. 3. Parameter regions where a planar film surface is unstable (above the solid line) and where stable periodic structures can form near the instability threshold (near the solid line, above the dashed line): (a) $\varepsilon=0.1$, $\gamma_s\delta^2/\nu=0.5$; (b) $\varepsilon=0.1$, $\gamma_s\delta^2/\nu=2.0$; (c) $\varepsilon=0.2$, $\gamma_s\delta^2/\nu=0.5$; and (d) $\varepsilon=0.4$, $\gamma_s\delta^2/\nu=0.5$.

B. Numerical simulations

We have performed numerical simulations of Eq. (26) for the two types of wetting potentials, by means of a pseudospectral code with the time integration in Fourier space using the Crank-Nicolson scheme for the linear operator and the Adams-Bashforth scheme for the nonlinear operator. Numerical solutions in both cases exhibited the formation of stable periodic structures near the instability threshold in the parameter regions where these structures are stable. At the same time, outside these regions or with the increase of the supercriticality, the periodic stationary structures become unstable and exhibit different behavior, depending on the type of wetting interactions. We have found that with the two-layer wetting potential (9)–(11), the surface mounds grow and coarsen (large islands grow at the expense of small ones), with the film between the islands getting thinner and thinner, until its thickness reaches zero in a finite time and then becomes negative, which is unphysical. This is clearly an artifact of the present *continuum* model, based on the conservation of mass, that neither treats the substrate as a separate surface with its own transport properties, nor can it properly describe the dynamics of a monolayer wetting film. Although zero film thickness may indicate dewetting, the latter process itself, on the one hand, cannot be described within the framework of this model, and, on the other hand, is not the focus of the present investigation aimed at studying systems in which the film between the islands evolves to small thickness but never exposes the substrate. The persistence of a very thin, "glued" wetting layer, typical of the Stranski-Krastanov growth, indicates a very large energy penalty for its removal. Such energy barrier can be effectively described by the phenomenological glued-layer model (12) in which the wetting potential is singular for $h\to 0$ (see also Refs. 28 and 29).

In Figs. 4 and 5 we present the results of the numerical simulations of Eq. (26) with the wetting potential corre-

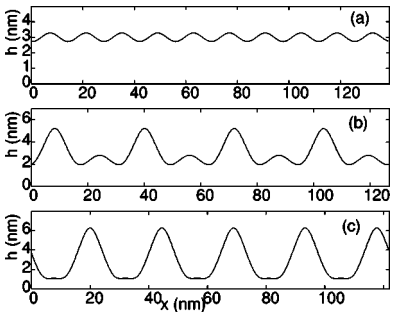

FIG. 4. Stationary numerical solutions of Eq. (26) with the wetting potential (12) showing stationary surface structures for $h_0=3.0$ nm, ($\zeta=2.0$), $a=0.17$ J m^{-2}, and (a) $w=6.8\times10^8$ J m^{-3} ($w_{01}=0.24$); (b) $w=2.8\times10^8$ J m^{-3} ($w_{01}=0.1$); and (c) $w=2.8\times10^7$ J m^{-3} ($w_{01}=0.01$).

sponding to the glued wetting-layer model defined by (12). The shown length scales correspond to the following parameter values, typical of semiconductors like Si or Ge: $\gamma\sim2.0$ J m^{-2}, $\sigma\sim0.2$ J m^{-2}, $\delta\sim1.5$ nm, and the estimates of $\alpha=3.0$ and $\nu\sim\gamma a_0^2\sim5.0\times10^{-19}$ J, where $a_0\sim0.5$ nm is the crystal lattice spacing; the nonlinear coefficient of the surface-energy anisotropy, a, the initial film thickness, h_0, and the wetting interaction strength parameter, w, are varied. In experiment, the film thickness is the main parameter that controls the film instability. For example, for $w\sim\Delta\gamma/\delta\sim6.7\times10^7$ J m^{-3}, where $\Delta\gamma\sim0.1$ J m^{-2} is the surface-tension difference between the substrate and the film, one finds that if the initial film thickness, h_0, ranges from 1.2 to 5.3 nm, the parameter w_{01} changes from 2.3 to 7.3 $\times10^{-4}$, respectively. The instability occurs in this case for a film thicker than $h_0\approx1.9$ nm, and the wavelength of the structure at the onset of instability is 14.0 nm.

Figure 4 presents the stationary solutions of Eq. (26) for different values of the dimensionless wetting parameter, w_{01}, corresponding to different values of the wetting interaction strength, w, and the initial film thickness, h_0. One can see that, near the instability threshold, an almost harmonic small-amplitude periodic structure is formed. Farther from the threshold, the formation of periodic structures with larger amplitude and larger wavelengths can be observed. In the

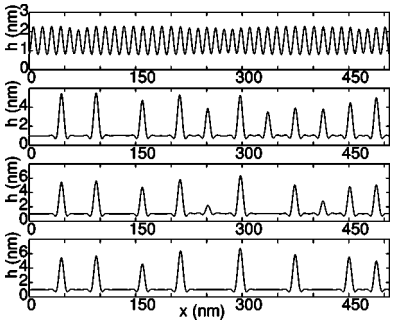

FIG. 5. Different stages of coarsening of the initial periodic structure, yielding the formation of localized dots divided by a thin wetting layer—the numerical solution of Eq. (26) with the wetting potential (12); $h_0=1.5$ nm, $w=8.2\times10^6$ J m^{-3} ($\zeta=1.0, w_{01}=0.1$), $a=0.22$ J m^{-2}.

parameter regions where a near-threshold periodic structure with the wavelength corresponding to the most rapidly growing linear mode is unstable, it undergoes coarsening right after formation, and finally evolves into spatially *localized* dots. Different stages of this coarsening process and the formation of localized islands are shown in Fig. 5. At the last stage, shown in Fig. 5, the coarsening either completely stops or becomes logarithmically slow.

Thus, the presence of wetting interactions between the film and the substrate can suppress the faceting instability of the film surface, that is thermodynamically unstable due to strong anisotropy of the surface energy, and lead to the formation of spatially regular surface structures, or to the formation of spatially localized dots divided by a thin wetting layer. In the next section we consider evolution of a more realistic, 2+1 system.

V. FORMATION OF SURFACE STRUCTURES: 2+1 CASE

In this section we investigate the nonlinear evolution of surface structures resulting from the faceting instability of a three-dimensional film with a two-dimensional surface (2+1 case) in the presence of wetting interactions with the substrate. We consider high-symmetry orientations only, [001] and [111], described by Eq. (15).

After the appropriate rescaling, Eq. (15) can be written as

$$\partial_t h=\Delta\{\Delta h+\Delta^2 h-g[h]+w_0(h)+w_2(h)(\nabla h)^2+w_3(h)\Delta h\}, \tag{45}$$

where the nonlinear differential operator $g[h]$ for [001] orientation is

$$g_{001}=(h_x^2+ph_y^2)h_{xx}+(h_y^2+ph_x^2)h_{yy}+4ph_xh_yh_{xy}, \tag{46}$$

and for [111] orientation it is

$$g_{111}=\left(h_x^2+\tfrac{1}{3}h_y^2\right)h_{xx}+\left(h_y^2+\tfrac{1}{3}h_x^2\right)h_{yy}+\tfrac{4}{3}h_xh_yh_{xy}+q[(h_{xx}-h_{yy})h_y+2h_{xy}h_x]. \tag{47}$$

Equation (45) has a special structure in that the linear operator is isotropic, while the nonlinear operator is anisotropic. The linear growth rate near the instability threshold, thus, does not depend on the wave vector orientation and the resulting dispersion relation is the same as in the 1+1 case, $\omega=-w_{01}k^2+k^4-k^6$, with the instability threshold $w_{01}=\frac{1}{4}$ at $k=k_c=\sqrt{2}/2$. It is the nonlinear interaction between the modes that will determine the symmetry of the emerging pattern. This situation is similar to the one considered in Ref. 32 where the effect of surface-energy anisotropy on the formation of cellular patterns with different symmetries at a crystal-melt interface caused by morphological instability during directional solidification was studied. In the next section we consider the weakly nonlinear analysis near the instability threshold.

A. Weakly nonlinear analysis

Since the linear operator of Eq. (45) is isotropic and the nonlinear operator of Eq. (45) has a quadratic nonlinearity that breaks $h\rightarrow-h$ symmetry, the preferred pattern near the

instability threshold will have a *hexagonal* symmetry, caused by the quadratic resonant interaction between three different modes oriented at 120° with respect to one another and having the same linear growth rate. The specific type of pattern in this case is determined by the phase locking of the three resonant modes that depends on the quadratic resonant interaction coefficient. In order to compute this coefficient, take $w_{01}=\frac{1}{4}-2\gamma\epsilon$, $\epsilon\ll 1$, introduce the slow time $\tau=\epsilon t$, and use the expansions (28)–(30), as well as the expansion

$$h=\epsilon\sum_{n=1}^{3}A_n(\tau)e^{\mathbf{k}_n\cdot\mathbf{r}}+\epsilon^2\sum_{n=1}^{3}B_n(\tau)e^{\mathbf{k}_n\cdot\mathbf{r}}+\epsilon^2\sum_{n=1}^{3}[B_{n,n}(\tau)e^{2\mathbf{k}_n\cdot\mathbf{r}}+B_{n,n-1}(\tau)e^{(\mathbf{k}_n-\mathbf{k}_{n-1})\cdot\mathbf{r}}]+\text{c.c.}+O(\epsilon^3), \tag{48}$$

where $A_n(\tau)$, $B_n(\tau)$, $B_{n,n}(\tau)$, and $B_{n,n-1}(\tau)$ are complex amplitudes (the spatially uniform mode $B_{n,-n}$ is missing due to the conservation of mass), $\mathbf{r}$ is a vector in the (x,y) plane, $k_n=1/\sqrt{2}$ and $\mathbf{k}_1+\mathbf{k}_2+\mathbf{k}_3=0$ ($n=0$ and $n=3$ correspond to the same mode with the wave vector $\mathbf{k}_3$). Then, the solvability condition for the problem for B_n in the order ϵ^2 yields the following three evolution equations for the amplitudes $A_{1,2,3}$:

$$\partial_\tau A_1=\gamma A_1+\alpha A_2^* A_3^*, \tag{49}$$

where the other two equations are obtained by the cyclic permutation of the indices in Eq. (49). The resonant quadratic interaction coefficient is different for different surface orientations:

$$\alpha^{001}=\tfrac{3}{4}w_{20}-w_{02}, \tag{50}$$

$$\alpha^{111}=\alpha^{001}-i\frac{q}{4\sqrt{2}}\sin 3\phi_0, \tag{51}$$

where the angle ϕ_0 characterizes the orientation of the resonant triad $\{\mathbf{k}_1,\mathbf{k}_2,\mathbf{k}_3\}$ in the surface plane, $\mathbf{k}_1=(\cos\phi_0,\sin\phi_0)$. Thus, in the case of the [001] surface, the quadratic mode interaction is isotropic, while in the case of [111] surface it depends on the pattern orientation within the [111] plane.

For equilateral patterns $A_k=\rho e^{i\theta_k}$ and using $\alpha=|\alpha|e^{i\delta}$ one obtains from (49) the following system of equations for ρ and $\Theta=\theta_1+\theta_2+\theta_3$:

$$\partial_\tau\rho=\gamma\rho+|\alpha|\rho^2\cos(\Theta-\delta), \tag{52}$$

$$\partial_\tau\Theta=-3\rho|\alpha|\sin(\Theta-\delta). \tag{53}$$

Equation (53) has two critical points: stable, $\Theta=\delta$, and unstable, $\Theta=\pi+\delta$. Thus, the system (52) and (53) describes an unbounded growth of a pattern given by a function

$$h=\rho[\cos(\mathbf{k}_1\cdot\mathbf{x}+\theta_1)+\cos(\mathbf{k}_2\cdot\mathbf{x}+\theta_2)+\cos(\mathbf{k}_3\cdot\mathbf{x}+\theta_3)], \tag{54}$$

in which the phases are locked: $\theta_1+\theta_2+\theta_3=\delta$. If the resonant interaction coefficient is real, then $\delta=0$ ($\alpha>0$) or $\delta=\pi$ ($\alpha<0$), and the function (54) describes a spatially regular array of hexagons with $h>0$ ($h<0$) in the centers of the hexagons for $\alpha>0$ ($\alpha<0$). Therefore, in the case of the [001] surface when α^{001} is real, one could observe the growth of regular hexagonal arrays of dots for $\alpha^{001}>0$ or pits for $\alpha^{001}<0$. Note that for [001] orientation, the pattern type is determined purely by the details of the wetting potential (the coefficients w_{02} and w_{20}) since in this case the anisotropic surface energy enters only through the quartic terms in the free energy functional yielding cubic nonlinear terms in the evolution equation for the surface shape. For example, for a glued wetting potential of type (12), $w_{20}=0$, $\alpha^{001}=-w_{02}>0$ and therefore the formation of only hexagonal arrays of *dots* is possible, an array of pits cannot form.

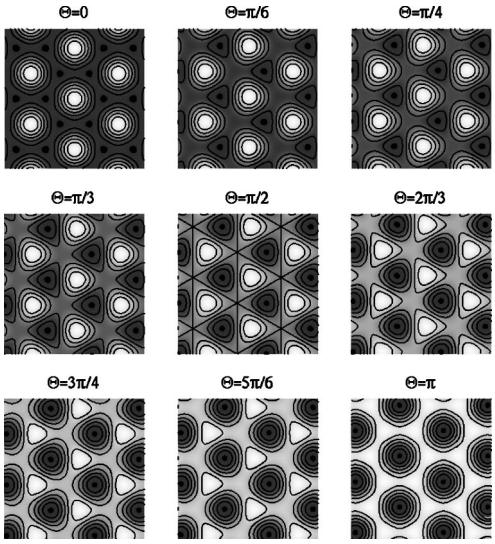

FIG. 6. Spatial patterns described by (54) with different values of $\Theta=\theta_1+\theta_2+\theta_3$.

The situation is different for [111] orientation when the free-energy functional has anisotropic cubic terms leading to anisotropic quadratic terms in the evolution equation for the surface shape and the complex quadratic resonant interaction coefficient. In this case, the imaginary part of the resonant interaction coefficient depends on the surface-energy anisotropy coefficient, q, and the pattern orientation within the [111] plane (angle ϕ_0). As one can see from (52), the most rapidly growing pattern corresponds to the maximum of $|\alpha|$ that is achieved for $\phi_0=\pi/6$. Thus, one would observe in this case the growth of a pattern described by the function (54) with the phases locked at

$$\Theta=\arctan\left[\frac{q/\sqrt{2}}{4w_{02}-3w_{20}}\right]. \tag{55}$$

Examples of patterns corresponding to different values of Θ are shown in Fig. 6 (see also Ref. 32). One can see that for intermediate values of Θ the growing pattern consists of a regular hexagonal array of triangular pyramids. Note that similar hexagonal arrays of triangular pyramids were observed in experiments reported in Ref. 33. Although the physical mechanism of the formation of ordered arrays of triangular pyramids observed in Ref. 33 was different (elastic interaction of multiple epitaxial layers), the *nonlinear mechanism* based on the resonant quadratic interaction of unstable modes in the presence of the anisotropy of the [111]

orientation is universal and may well be the same in the system studied in Ref. 33.

The amplitude equations (49) cannot describe the nonlinear stabilization of a growing surface structure and cannot provide conditions for the formation of stable, spatially regular structures near the instability threshold. In order to obtain such conditions higher order (usually cubic) nonlinear terms in the amplitude equations need to be taken into account. However, in the presence of the resonant quadratic interaction, the addition of cubic terms in the amplitude equations near the instability threshold is asymptotically rigorous only if the quadratic interaction coefficient is small, $|\alpha| \sim \epsilon$, which restricts the validity of the weakly nonlinear analysis to a narrow range of physical parameters. The Landau cubic interaction coefficients will be anisotropic and depend on the pattern orientation in the surface plane.[32] Besides, if one allows for long-scale spatial modulations of the patterns, the interaction between the unstable periodic modes and the Goldstone mode will strongly affect the pattern stability (see Sec. IV) and must be taken into account. The resulting system of amplitude equations with cubic terms, coupled to an equation for the Goldstone mode, will be similar to that studied in Ref. 16, but will have anisotropic Landau coefficients and anisotropic and complex quadratic coefficients. The full stability analysis of such a system is cumbersome; it is beyond the scope of the present paper and will be done elsewhere. In this paper we rather perform numerical simulations of the full 2D nonlinear evolution equation (45) for the two orientations of the film free surface. The results of the numerical simulation are described in the next section.

B. Numerical simulations

We have performed numerical simulations of Eq. (15) for the two orientations of the film surface: [001] and [111], with $\Gamma_{ijk}[h]$ defined by (16) and (17), respectively, and for the glued-layer wetting potential $W_0(h)$ defined by (12) [so that $W_2(h) = W_3(h) = 0$ in (15)]. We have used a pseudospectral 2D code similar to the 1D code described in Sec. IV. We have considered two different cases: formation of structures during surface annealing and during ballistic deposition.

1. Structure formation during surface annealing

If the initial film thickness h_0 is so large that the film does not "feel" the substrate, $h_0 \gg \delta$, the numerical solutions of Eq. (45) exhibit the formation of "faceted" pyramidal structures (square pyramids for [001] surface and triangular pyramids for [111] surface) that coarsen in time, similar to those described in Refs. 7 and 15. If the film is thin enough so that the wetting interactions become important, in the case of [001] surface one can observe the formation of spatially regular (with some defects), hexagonal arrays of rounded dots. We have observed that these arrays of equal-sized dots can be stable for small supercriticality and large enough surface-energy anisotropy [large enough coefficient a together with the ratio a/b in Eq. (15)]. An example of such stable array is shown in Fig. 7(a). It is interesting that the surface-energy anisotropy is overcome here by the isotropic wetting interactions. With the increase of the supercriticality

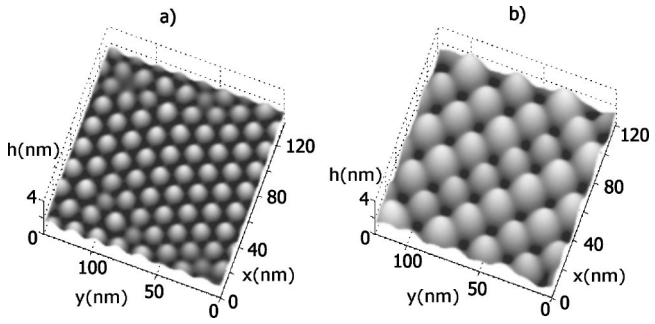

FIG. 7. Formation of spatially regular arrays of dots: numerical solutions of Eq. (15) for [001] surface orientation. (a) Stationary hexagonal array of equal-size dots, $h_0 = 1.5$ nm, $w = 1.89 \times 10^7$ J m^{-3}, $a = 6.6$ J m^{-2} ($w_{01} = 0.23, \zeta = 1.0$). (b) Stationary square array of equal-size dots, $h_0 = 1.5$ nm, $w = 8.2 \times 10^5$ J m^{-3}, $a = 11.1$ J m^{-2} ($w_{01} = 0.01, \zeta = 1.0$); Other parameters are the same as in Figs. 4 and 5 and $b = 0$.

and further increase of the surface-energy anisotropy, formation of spatially regular square arrays of equal-sized dots shown in Fig. 7(b) is possible. If the anisotropy coefficient a is not sufficiently large, hexagonal arrays of dots that are formed at the initial stage of the film instability [Fig. 8(a)] coarsen in time, resulting in the formation of rounded localized dots shown in Fig. 8(b). These dots are connected with each other by a thin wetting layer. The mound slope remains constant during the coarsening. At the late stages, when the dots become localized, the coarsening rate decreases sharply and the coarsening apparently stops.

In the case of the [111] orientation of the film surface we have not observed the formation of regular arrays of dots even near the instability threshold and for large surface-tension anisotropy coefficients. For all studied parameter values we have observed the initial formation of a hexagonal array of triangular pyramids that further coarsen and evolve towards localized triangular pyramidal structures; different stages of the coarsening process are shown in Fig. 9. As the localized dots shown in Fig. 8(b), the localized pyramids here are divided from one another by a thin wetting layer and at the late stages the coarsening apparently stops. It is interesting that, unlike [001] surface orientation, the localized

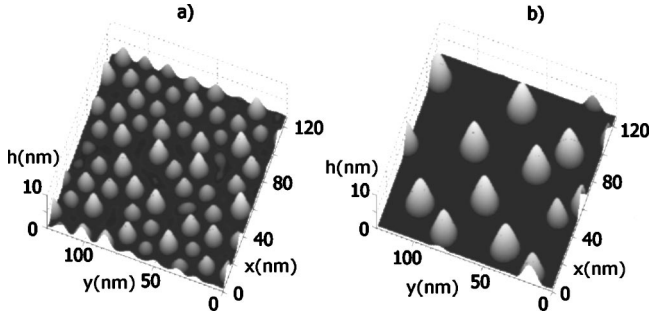

FIG. 8. Formation of localized dots via coarsening: numerical solutions of Eq. (15) for [001] surface orientation. (a) Nearly hexagonal array of dots (initial stage); (b) spatially localized dots divided by a thin wetting layer (late stage); $h_0 = 1.5$ nm, $w = 8.2 \times 10^6$ J m^{-3}, $a = 0.22$ J m^{-2} ($w_{01} = 0.1, \zeta = 1.0$). Other parameters are the same as in Figs. 4 and 5 and $b = 0$.

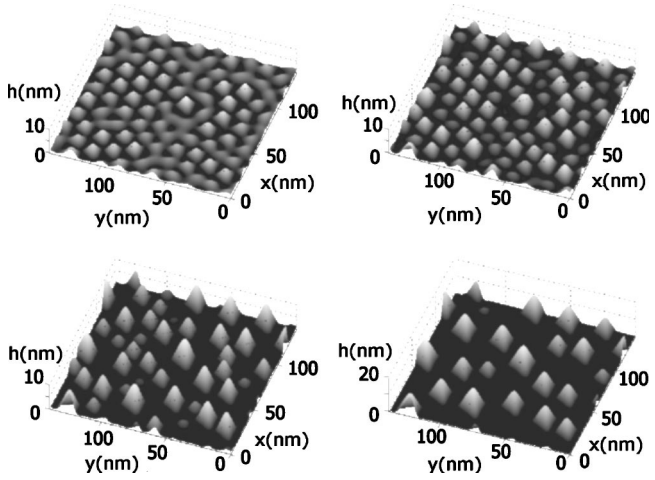

FIG. 9. Formation of localized dots: numerical solutions of Eq. (15) for [111] surface orientation showing different stages of coarsening of initial regular hexagonal array of triangular pyramids. The parameters are the same as in for the case shown in Fig. 8, except $b=0.44$ J m^{-2}.

dots grown on [111] surface are strongly anisotropic. This is due to anisotropic cubic terms in the free energy functional (anisotropic quadratic terms in the evolution equation) that in the small slope approximation become dominant. Note that self-organization of quantum dots in the form of localized triangular pyramids on a [111] surface was observed in Ref. 34. Although in experiments described in Ref. 34 an elastic mechanism of the solid film instability seems to play an important role, the triangular shape of the pyramids with [001] faces is clearly caused by the anisotropic surface energy, which is correctly captured by our model.

2. Structure formation during ballistic deposition

Finally, it is interesting to study the effect of the film growth by ballistic deposition on the formation of surface structures caused by the interplay between the anisotropic surface energy and the wetting interactions between the film and the substrate. One can expect that if the surface evolution is accompanied by ballistic deposition, the influence of wetting interactions will decay with the film growth, and the anisotropic effects of surface energy will become more pronounced. The effect of the film growth by ballistic deposition can be described by adding a constant deposition rate term, $V=$const, to the right-hand side of Eq. (15). As an example, we have chosen the [001] surface orientation of the film since in this case the cubic nonlinear effects of anisotropic surface energy are almost completely suppressed by quadratic nonlinearity of isotropic wetting interactions.

We have performed numerical simulations of Eq. (15) for [001] surface with an additional constant deposition rate term. The result is shown in Fig. 10. One can see that, indeed, in the course of the film growth, when the film becomes thicker, the effects of wetting interactions decay and the rounded localized surface mounds become anisotropic and acquire pyramidal shape, as in the case of faceting instability of thermodynamically unstable crystal surfaces.[7,15] Also, we have observed that the growth of the film is accompanied by the coarsening of the pyramidal structures, as in the case of annealing of thermodynamically unstable surface, and the rate of coarsening does not depend on the deposition rate. Indeed, for thick enough films, when the wetting interactions decay and become negligible, the only order parameter that governs the dynamics of the surface structures is the local surface slope, and the effect of the film growth is eliminated in the frame of reference moving with the mean surface position. This is different from the faceting instability accompanied by the film growth by the evaporation-condensation mechanism that produces the flux normal to the film surface.

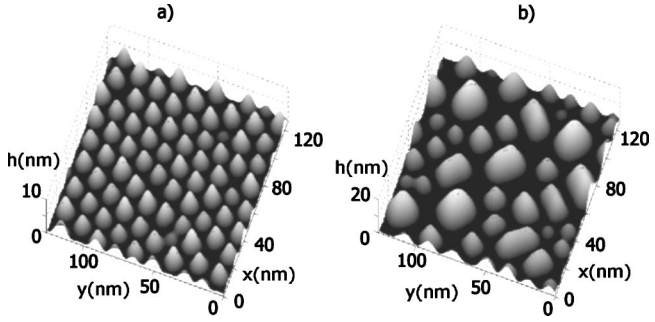

FIG. 10. Evolution of dots accompanied by ballistic deposition: numerical solutions of Eq. (15) in 2D with the additional constant deposition term. (a) Hexagonal array of equal-size dots (initial stage); (b) larger dots with pyramidal shape (later stage); $h_0=1.5$ nm, $w=8.2\times10^6$ J m^{-3}, $a=0.22$ J m^{-2} ($w_{01}=0.1, \zeta=1.0$), deposition rate $V=0.2$ nm/min. Other parameters are the same as in Fig. 1 and $b=0$.

VI. EFFECT OF EPITAXIAL STRESS

The analysis presented above assumes that the epitaxial stress in the film is negligible and the instability is driven solely by the anisotropic surface energy. In experimental heteroepitaxial systems, however, the epitaxial stress is always present. It is instructive to estimate the effect of epitaxial stress on the surface-energy-driven mechanism of instability.

The effect of epitaxial stress is always destabilizing. The analysis of the ATG instability in a thin solid film in the presence of wetting interactions with the substrate has been done in Refs. 16 and 19. In the linear, small-slope approximation, the effect of the anisotropic surface energy will be additive to the effect of stress. Thus, one can just add the corresponding terms from the dispersion relation (22) to the dispersion relation obtained in Ref. 19 for the general case of an elastic substrate to obtain

$$\mathcal{D}^{-1}\omega = -W_{01}k^2 + B_3k^3 + (\sigma + B_4)k^4 - B_5k^5 - (B_6 + \nu)k^6,$$

where the coefficients B_i are proportional to the square of the lattice misfit, ε^2, and depend on the elastic constants of the film and the substrate. For example, for a rigid substrate,

$$B_3 = B_5 = 0,$$

$$B_4 = \frac{4\varepsilon^2 h_0 \mu^f (1+p)^2}{(1-p)^2}, \tag{56}$$

$$B_6 = 2\varepsilon^2 h_0^3 \mu^f (3+4p)(1+p)^2,$$

and, for an elastic substrate with the shear modulus close to that of the film,

$$B_3 = \frac{4\varepsilon^2 \mu^f (1+p)^2}{1-p},$$

$$B_4 = B_5 = B_6 = 0, \tag{57}$$

where h_0 is the initial film thickness, μ^f is the shear modulus of the film and p is its Poisson ratio.

One can see that the presence of the epitaxial stress merely shifts the critical value of the wetting interaction coefficient, W_{01}^c, corresponding to the onset of the instability, as well as the threshold wave number of the emerging periodic structure, k_c. In the case of a rigid substrate,

$$W_{01}^c = \frac{B_4^2}{4B_6}, \quad k_c^2 = \frac{\sigma + B_4}{2\nu + B_6},$$

and for small epitaxial stress, one obtains

$$W_{01}^c = \frac{\sigma^2}{4\nu}[1 + \varepsilon^2 h_0 \mu^f (8P_1 - 2P_2)],$$

$$k^c = \sqrt{\frac{\sigma}{2\nu}}[1 + \varepsilon^2 h_0 \mu^f (2P_1 - P_2)],$$

where

$$P_1 = \sigma^{-1}\left(\frac{1+p}{1-p}\right)^2, \quad P_2 = \frac{h_0^2}{\nu}(3+4p)(1+p)^2.$$

Thus, in the case of a rigid substrate, the shift of the critical value of the wetting interaction coefficient and of the critical wave number can be of either sign, depending on the Poisson ratio, surface stiffness, regularization coefficient and the initial film thickness.

In the case of an elastic substrate whose shear modulus is close to that of the film, for small epitaxial stress, one obtains

$$W_{01}^c = \frac{\sigma^2}{4\nu} + B_3 k_0,$$

$$k_c = k_0 + \frac{B_3}{4\sigma},$$

where $k_0 = \sqrt{\sigma/(2\nu)}$ and B_3 is defined by (57). Thus, in this case the critical value of the wetting parameter as well as the critical wave number are slightly increased due to the presence of a small epitaxial stress.

Note that in a recent paper[17] fully nonlinear numerical simulations of the dynamics of the *stress-driven* instability in the presence of wetting interactions and anisotropic surface energy, governed by surface diffusion, have been performed. The formation of spatially regular arrays of square pyramids has been observed for some parameter values.

VII. CONCLUSIONS

In conclusion, we have found that, besides the stress-driven instability, there can be another mechanism of the formation of quantum dots in epitaxially grown thin solid films. By this mechanism, the substrate determines that the film surface grows in a specific crystallographic orientation. In the case of a thick film that does not feel the substrate, this orientation would be forbidden, (i.e., thermodynamically unstable), leading to the formation of faceted structures. Wetting interactions between the film and the substrate suppress the long-wave modes of this instability and change its spectrum from the spinodal decomposition type to the Turing type, thus yielding a possibility of the self-organization of stable, spatially regular hexagonal or square arrays of equal-size dots. We have shown also that, depending on the initial orientation of the film surface, this type of surface instability can lead to the formation of rounded dots whose coarsening apparently stops when they become localized (in the case of the [001] surface), or to the formation of localized faceted triangular pyramids (in the case of the [111] surface). This difference is explained by the presence of cubic anisotropic terms in the surface free energy in the case of the [111] orientation. We have found the parameter regions in which, depending on the type of wetting interactions, one can observe the formation of stable periodic arrays of dots. In the presence of deposition, or for sufficiently thick films, the dots can acquire pyramidal shape due to the decrease of the effect of isotropic wetting interactions. This new mechanism can provide a new route for producing self-organized quantum dots. Small epitaxial stresses would not change this mechanism qualitatively, but merely lead to a small shift of the critical film thickness, critical wetting parameter and the threshold wave number.

Note that spatially regular stable arrays of dots caused by wetting interactions exist in a rather narrow range of parameters, bounded by proximity to the instability threshold and by the stability interval determined by the interaction with the Goldstone mode. Therefore, experimental implementation of the conditions that may lead to the self-assembly of spatially regular arrays of dots can be a challenge for experimentallists.

ACKNOWLEDGMENTS

The authors are grateful to Professor Peter W. Voorhees for numerous fruitful discussions. This work was supported by the National Science Foundation Grant No. DMR-0102794.

[1] R. J. Asaro and W. A. Tiller, Metall. Trans. **3**, 1789 (1972); M. Y. Grinfeld, Sov. Phys. Dokl. **31**, 831 (1986).
[2] V. A. Shchukin and D. Bimberg, Rev. Mod. Phys. **71**, 1125 (1999).
[3] D. J. Srolovitz, Acta Metall. **37**, 621 (1989).
[4] B. J. Spencer, P. W. Voorhees, and S. H. Davis, Phys. Rev. Lett. **67**, 3696 (1991).
[5] Y. W. Zhang, Phys. Rev. B **61**, 10388 (2000); Y. W. Zhang and A. F. Bower, Appl. Phys. Lett. **78**, 2706 (2001); P. Liu, Y. W. Zhang, and C. Lu, Phys. Rev. B **68**, 035402 (2003).
[6] J. Stewart and N. Goldenfeld, Phys. Rev. A **46**, 6505 (1992); F. Liu and H. Metiu, Phys. Rev. B **48**, 5808 (1993).
[7] A. A. Golovin, S. H. Davis, and A. A. Nepomnyashchy, Phys. Rev. E **59**, 803 (1999).
[8] M. Siegert and M. Plishke, Phys. Rev. Lett. **73**, 1517 (1994); M. Siegert, *ibid.* **81**, 5481 (1998).
[9] P. Smilauer, M. Rost, and J. Krug, Phys. Rev. E **59**, R6263 (1999).
[10] D. Moldovan and L. Golubovic, Phys. Rev. E **61**, 6190 (2000).
[11] F. M. Ross, J. Tersoff, and R. M. Tromp, Phys. Rev. Lett. **80**, 984 (1998).
[12] K. Alchalabi, D. Zimin, G. Kostorz, and H. Zogg, Phys. Rev. Lett. **90**, 026104 (2003).
[13] C. D. Rudin and B. J. Spencer, J. Appl. Phys. **86**, 5530 (1999).
[14] A. A. Golovin, A. A. Nepomnyashchy, S. H. Davis, and M. A. Zaks, Phys. Rev. Lett. **86**, 1550 (2001).
[15] T. V. Savina, A. A. Golovin, S. H. Davis, A. A. Nepomnyashchy, and P. W. Voorhees, Phys. Rev. E **67**, 021606 (2003).
[16] A. A. Golovin, S. H. Davis, and P. W. Voorhees, Phys. Rev. E **68**, 056203 (2003).
[17] C. Chiu, Phys. Rev. B **69**, 165413 (2004).
[18] H. R. Eisenberg and D. Kandel, Phys. Rev. Lett. **85**, 1286 (2000); Phys. Rev. B **66**, 155429 (2002).
[19] T. V. Savina, P. W. Voorhees, and S. H. Davis, J. Appl. Phys. **96**, 3127 (2004).
[20] M. Ortiz, E. A. Repetto, and H. Si, J. Mech. Phys. Solids **47**, 697 (1999).
[21] P. Nozieres, in *Solids far from Equilibrium*, edited by C. Godrèche (Cambridge University Press, Cambridge, 1992).
[22] A. Pimpinelli and J. Villain, *Physics of Crystal Growth* (Cambridge University Press, Cambridge, 1998).
[23] B. J. Spencer, P. W. Voorhees, and S. H. Davis, J. Appl. Phys. **73**, 4955 (1993).
[24] M. E. Gurtin, *Thermomechanics of Evolving Phase Boundaries in the Plane* (Clarendon, Oxford, 1993).
[25] C. H. Chiu and H. Gao, in *Thin Films: Stresses and Mechanical Properties V*, edited by S. P. Baker *et al.*, MRS Symposia Proceedings No. 356 (Materials Research Society, Pittsburgh, 1995), p. 33.
[26] J. Tersoff, Phys. Rev. B **43**, 9377 (1991).
[27] M. J. Beck, A. Van de Walle, and M. Asta, Phys. Rev. B (to be published).
[28] Z. Suo and Z. Zhang, Phys. Rev. B **58**, 5116 (1998).
[29] B. J. Spencer, Phys. Rev. B **59**, 2011 (1999).
[30] D. Walgraef, *Spatio-Temporal Pattern Formation* (Springer, New York, 1997).
[31] P. C. Matthews and S. M. Cox, Nonlinearity **13**, 1293 (2000).
[32] R. B. Hoyle, G. B. McFadden, and S. H. Davis, Philos. Trans. R. Soc. London, Ser. A **354**, 2915 (1996).
[33] G. Springholtz, V. Holy, M. Pinczolits, and G. Bauer, Science **282**, 734 (1998); M. Pinczolits, G. Springholtz, and G. Bauer, Phys. Rev. B **60**, 11524 (1999).
[34] K. Alchalabi, D. Zimin, G. Kostorz, and H. Zogg, Phys. Rev. Lett. **90**, 026104 (2003).